REVISTA INTERDISCIPLINAR DE PESQUISA EM ENGENHARIA

CILAMCE 2016

XXXVII IBERIAN LATIN AMERICAN CONGRESS ON COMPUTATIONAL METHODS IN ENGINEERING
BRASÍLIA - DF - BRAZIL

A STAGGERED SCHEME WITH ADAPTIVE TIME STEP CONTROL FOR FLUID-STRUCTURE INTERACTION

Thomas Miras

Fernando A. Rochinha

Alvaro L.G.A. Coutinho

thomas.miras@nacad.br

High Performance Computing Center and Mechanical Engineering Department - Federal University of Rio de Janeiro (UFRJ)

Av. Horácio Macedo, 2030 - Centro de Tecnologia - Ilha do Fundão - Caixa Postal 68516, Rio de Janeiro, RJ - CEP 21941-598 - Brasil

Abstract. *The coupling between a rigid body and an incompressible fluid is investigated. Within the framework of ALE, we use a residual-based variational multiscale (RBVMS) formulation to solve the incompressible Navier Stokes equations. Mesh updating is accomplished by a parallel edge-based solution of a non-homogeneous scalar diffusion problem in each spatial coordinate. This work is in the continuation of previous results presented in Miras et al. (2015). We use here a staggered type of coupling with a prediction/correction approach for the forces applied on the rigid body. A time stepping by a Proportional-Integral-Derivative controller based on the CFL number is also presented. The coupling approach is tested on different cases coming from the literature and in the area of Vortex Induced Vibrations (VIV), allowing to evaluate the performance of the method in term of accuracy and robustness. We give particular attention to the parameters used to compute the force/moment prediction.*

Keywords: *Fluid-Object-Interaction, ALE, Vortex Induced Vibration, Time Step Control*

1 INTRODUCTION

In the context of Fluid-Object Interaction (FOI), offshore engineering and marine renewable energy systems present a wide range of complex problems including Vortex Induced Vibrations (VIV). Structures such as risers, pipelines or marine current devices can experience VIV and the interaction with an incompressible fluid is of interest. In some cases, consequences of the liquid movements can be dramatic and the understanding of the interaction phenomenon helps designing VIV suppression devices Tumkur et al. (2013), or can help developing techniques to capture the flow energy Day et al. (2015); Sung et al. (2015). Thus, there exists a need to understand and estimate the interaction between the structure and the incompressible liquid. With this in mind we can, in particular, cite the important works done in Fluid-Structure Interaction (FSI) and Fluid-Object Interactions (FOI) by Donea and Huerta (2003), Bazilevs, Takizawa and Tezduyar (2013) or Hughes (2012). The variational multiscale method (VMS) Hughes et al. (1998), provides a theoretical framework for general multiscale problems in computational mechanics by separating the scales of interest in a predetermined number of groups (usually two, coarse and fine scales). This approach has been applied successfully to a number of turbulent flow problems, with different discretization methods. See Bazilevs et al. (2007), Calo (2004), Calderer and Masud (2012), and Rasthofer and Gravemeier (2013). For FOI problems with a single fluid, moving mesh methods within the framework of the Arbitrary Lagrangian Eulerian (ALE) method, are often preferred when large rigid body motions have to be taken into account. We do not give details about this method here, but we rather refer the interested reader to the literature that describes the method or addressing attention to a particular aspect of the overall methodology: Calderer and Masud (2010); Löhner (2008); Souli and Benson (2013). We focus here on the interaction between the rigid body and the fluid, and the time integration of the governing equations of the rigid body dynamics. The results presented are in the continuity of previous works Elias et al. (2009); Lins et al. (2010). We extend the existing simulation capabilities with an implicit scheme, a Predictor/Corrector method adapted for time step control. Proportional-Integral-Derivative (PID) controllers are extensively used in canonical control applications Gustafsson, Lundh and Soderlind (1988). The advantageous performances of PID strategy for general coupled problems are presented in Valli, Carey and Coutinho (2002, 2005). Among the possible control forms we consider here the Courant-Friedrichs-Lewy number (CFL) that is directly linked with the time step calculation.

In section 2, we will first focus on the theoretical part presenting the equations of the different physical phenomena involved in the problem: the RBVMS finite element formulation, incompressible fluid flow, mesh displacement, and rigid body motion. The staggered time marching algorithm and the coupling setup are presented in section 3. These formulations are applied on different test cases in section 4 inspired from Hesch et al. (2014); Li, Sherwin and Bearman (2000); Robertson et al. (2003) to both validate and show the capabilities of the coupling method. A vibrating plate in an incompressible flow is first considered allowing the study of Vortex Induced Vibration problems for one degree of freedom only (rotation). It allows a comparison with different coupling methods and codes found in the literature and to evaluate the performances of the method in term of accuracy and robustness. This test case is then complexified considering 3 rotational degrees of freedom.

2 GOVERNING EQUATIONS

2.1 Incompressible Flow

The problem of interest involves the coupling between an incompressible Newtonian fluid and a rigid body, respectively governed by the Navier-Stokes equation and the Newton-Euler equations. The unknowns for the fluid are the velocity and pressure $(\mathbf{u},\, p)$ and the rotations and the displacements of the center of mass for the rigid body. The ALE approach introduces a new frame of reference, related to a moving space-time domain noted as $\Omega(t) \times \left[0,\, t_f\right]$, in which the Navier-Stokes equation is to be solved. We will consider here the RBVMS method. The weak formulation of the Navier Stokes equation for an incompressible fluid is given by:

$$\begin{aligned}
&\text{Find } (\mathbf{u},\, p) \in S_{\mathbf{u}} \times S_p \text{ such as } \forall\, (\mathbf{w},\, q) \in V_{\mathbf{u}} \times V_p \\
&\int_{\Omega} \rho \mathbf{w} \cdot \left(\frac{\partial \mathbf{u}}{\partial t} + (\mathbf{u} - \mathbf{u}_{mesh}) \cdot \nabla \mathbf{u} - \mathbf{b} \right) \mathrm{d}\Omega + \int_{\Omega} \epsilon\,(\mathbf{w}) : \sigma\,(p,\, \mathbf{u})\, \mathrm{d}\Omega = \int_{\Gamma_h} \mathbf{w} \cdot \mathbf{h}\, \mathrm{d}\Gamma \quad (1) \\
&\int_{\Omega} q\, \nabla \cdot \mathbf{u}\, \mathrm{d}\Omega = 0 \quad (2)
\end{aligned}$$

The weight spaces of functions are defined as $S_{\mathbf{u}} = \{\mathbf{u},\, \mathbf{u} \in H^1(\Omega)^3,\, \mathbf{u} = \mathbf{u}_E \text{ on } \Gamma_E \text{ and } \mathbf{u} = \dot{\mathbf{x}}_L \text{ on } \Gamma_L\}$ and $S_p = \{p,\, p \in L^2(\Omega),\, \int_\Omega p\, \mathrm{d}\Omega = 0\}$ for velocity and pressure along with their trial spaces counterparts $V_{\mathbf{u}}$ and V_p. $\mathbf{u}_{mesh}$ is the new reference frame velocity that is connected to the computational grid, $\mathbf{b}$ is the body force vector, and ρ the fluid density. Considering only Newtonian behavior, σ, the Cauchy stress tensor, is given by $\sigma\,(p, \mathbf{u}) = -p\mathbf{I} + 2\mu\epsilon\,(\mathbf{u})$ with $\mathbf{I}$ the identity, μ the dynamic viscosity and ϵ is the strain rate tensor. The natural boundary conditions can be written as:

$$\mathbf{u} = \mathbf{u}_E \quad \text{on } \Gamma_E, \qquad \mathbf{u} = \dot{\mathbf{x}}_L \quad \text{on } \Gamma_L, \qquad \sigma \cdot \mathbf{n} = \mathbf{h} \qquad \text{on } \Gamma_h$$

Γ_E is the fixed party of the boundary with respect to an inertial frame, Γ_L is the Lagrangian (moving) boundary, i.e., the moving rigid body surface, and $\mathbf{h}$ is the interaction traction force on Γ_h with $\mathbf{n}$ its outward normal vector. $\mathbf{u}_E$ and $\mathbf{x}_L$ are the fluid velocity on Γ_E and the Fluid-Object interface displacement on Γ_L. We have $\partial\Omega = \Gamma_E \cup \Gamma_L \cup \Gamma_h$. Employing RBVMS is twofold: obtain a stable and robust numerical method and to capture turbulence behavior without resorting to any sub-grid closure model. On the other hand, the sole use of RBVMS scales splitting for numerically model turbulence was advocated in Codina (2002) and its performance was analyzed into detail in Principe, Codina and Henke (2010). RBVMS methods rely on a scales splitting of the physical variables combined with variational projections. This splitting involving the large scales (those explicitly captured by the numerical grid) and the fine scales (subgrid scales) reads, for the present problem, as

$$\mathbf{u} = \mathbf{u}_h + \mathbf{u}' \quad \text{and} \quad p = p_h + p' \qquad (3)$$

The subscript h denotes the large scale component of the solution, while the superscript $'$ refers to the subgrid complement. The large scale component is directly associated with a finite element approximation considered over the partition of the domain into n_e elements Ω_e that are non-overlapping, with characteristic length h. We write $S_{\mathbf{u}} = S^h_{\mathbf{u}} \oplus S_{\mathbf{u}'}$ and $S_p = S^h_p \oplus S_{p'}$

with $(\mathbf{u}_h, \mathbf{u}^{'}, p_h, p^{'}) \in (S^h_{\mathbf{u}} \times S_{\mathbf{u}'} \times S^h_p \times S_{p'})$ and $(\mathbf{w}_h, \mathbf{w}^{'}, q_h, q^{'}) \in (S^h_{\mathbf{w}} \times S_{\mathbf{w}'} \times S^h_q \times S_{q'})$ the corresponding weight spaces. The fine-scales equations are given by:

$$p' = -\rho_F \tau_C R_C \quad \text{with} \quad R_C = \nabla \cdot \mathbf{u}_h$$
$$\mathbf{u}' = \tau_m \mathbf{R}_M \quad \text{with} \quad \mathbf{R}_M = \rho_F \left(\frac{\partial \mathbf{u}_h}{\partial t} + (\mathbf{u}_h - \mathbf{u}_{mesh}) \cdot \nabla \mathbf{u}_h - \mathbf{b}_h \right) - \nabla \cdot \sigma(\mathbf{u}_h, p_h)$$

R_C and $\mathbf{R}_M$ are respectively the residuals of the momentum and the incompressibility constraint equations. The parameters (τ_C, τ_M) are given by:

$$\tau_M = \left(\left(\frac{2}{\Delta t} \right)^2 + \left(c_1 \frac{\|\mathbf{u}_h - \mathbf{u}_{mesh}\|}{h_e} \right)^2 + \left(c_2 \frac{\nu}{h_e^2} \right)^2 \right)^{-\frac{1}{2}} \quad \text{and} \quad \tau_C = \frac{h_e}{3} \|\mathbf{u}_h - \mathbf{u}_{mesh}\| \tag{4}$$

h_e is the element length computed here simply as the cubic root of the element volume, Δt is the time step, ν the viscosity and (c_1, c_2) are mesh independent constants. Usually for linear elements we have $(c_1, c_2) = (2, 3)$. Finally, using the decomposition (3) into (2) we can obtain the following ALE-VMS method Bazilevs et al. (2012):

$$\begin{aligned}
&\text{Find } (\mathbf{u}_h, p_h) \in S^h_{\mathbf{u}} \times S^h_p \text{ such as } \forall (\mathbf{w}_h, q_h) \in V^h_{\mathbf{u}} \times V^h_p \\
&\text{Galerkin:} \begin{cases} \int_\Omega \rho_F \left(\frac{\partial \mathbf{u}_h}{\partial t} + (\mathbf{u}_h - \mathbf{u}_{mesh}) \cdot \nabla \mathbf{u} - \mathbf{b} \right) \cdot \mathbf{w}_h + \int_\Omega \epsilon(\mathbf{w}_h) : \sigma(p_h, \mathbf{u}_h) \\ - \int_{\Gamma_h} \mathbf{w}_h \cdot \mathbf{h} + \int_\Omega q_h \nabla \cdot \mathbf{u}_h \end{cases} \\
&\text{Stabilization:} \begin{cases} + \sum_1^{n_e} \int_{\Omega_e} \tau_M \left((\mathbf{u}_h - \mathbf{u}_{mesh}) \cdot \nabla \mathbf{w}_h + \frac{\nabla q_h}{\rho_F} \right) \cdot \mathbf{R}_M \\ + \sum_1^{n_e} \int_{\Omega_e} \rho_F \tau_C \nabla \cdot \mathbf{w}_h R_C \end{cases} \\
&- \sum_1^{n_e} \int_{\Omega_e} \tau_M \mathbf{w}_h \cdot (\mathbf{R}_M \cdot \nabla \mathbf{u}_h) - \sum_1^{n_e} \int_{\Omega_e} \frac{\nabla \mathbf{w}_h}{\rho_F} : \tau_M \mathbf{R}_M \otimes \tau_M \mathbf{R}_M = 0
\end{aligned} \tag{5}$$

The first part of equations (5) reproduce a standard Galerkin weak form. The second part can be interpreted as the stabilized finite element methods (SUPS/LSIC) Tezduyar (2007) and Tezduyar et al. (1992). The last row, on the other hand, features unusual terms arising from RBVMS formulation. As discussed into detail in Codina, Principe and Avila (2010) and Gravemeier and Wall (2011), they might be interpreted as numerical representations of the cross and Reynolds stresses arising in LES formulations, and, therefore, are used here as turbulence modeling.

2.2 Mesh Movement

An efficient mesh deformation computation is necessary to allow large motions of the object considered. Among the different options available for addressing node repositioning, we consider here the scheme proposed by Masud and Hughes (1997) and extended for three dimensional application in Masud, Bhanabhagvanwala and Khurram (2007) to compute the mesh displacement and velocity that is required to solve fluid equation (5). Nodes are repositioned as a result of the solution of the following scalar Boundary Value Problems, considering $\partial\Omega \cap \Gamma_L = \emptyset$::

$$\nabla \cdot ([1 + \tau_{mesh}] \nabla) x^i_N = 0 \quad / \, i \in [1, n_{sd}] \, , \mathbf{x}_N = \mathbf{x}_L \text{ on } \Gamma_L \, , \mathbf{x}_N = \mathbf{0} \text{ on } \partial\Omega \backslash \Gamma_L \tag{6}$$

n_{sd} is the number of space dimensions, $\mathbf{x}_N$ is the vector of nodal displacements and τ_{mesh} is an artificial diffusivity computed for each element e of the mesh according to formula (7).

$$\tau_{mesh}(e) = \frac{1 - V_{min}/V_{max}}{V_e/V_{max}} \tag{7}$$

The mesh velocity is deduced from $\mathbf{x}_N$ and $\mathbf{u}_{mesh} = \mathbf{x}_N/\Delta t$. V_{min}, V_{max} and V_e are respectively the least, the largest and the current volume in the mesh. τ_{mesh} has the crucial role of stiffening the elements in the immediate neighborhood of the body, allowing mesh distortion in the far field where large elements are usually located. The mesh movement BVP is discretized by a Galerkin finite element method. If the determinant used to compute the volume V_e is negative, the computation is halted since we consider that we have excessive mesh distortion.

2.3 Rigid Body Motions

The configuration assumed by a rigid body along the motion is described by the position of its center of mass $\mathbf{x}$ and a rotation operator $\mathbf{R}$(t). Indeed, the motion is decomposed into a translational displacement, a vector field in the three-dimensional Euclidean space $\mathbf{E}^3$, and a rotational component, which is represented by an orthogonal matrix that relates a fixed inertial frame to the one attached to the center of mass of the body. This rotation matrix $\mathbf{R}$ belongs to the special orthogonal group $SO(3) = \left\{\mathbf{R} : \mathbf{E}^3 \to \mathbf{E}^3 \text{ linear } \mathbf{R}^{\mathrm{T}}\mathbf{R} = \mathbf{I},\ \det(\mathbf{R}) = 1\right\}$. The dynamics of a rigid body is governed by the Newton-Euler equations:

$$m\mathbf{a} = \mathbf{f} \tag{8}$$

$$\dot{\mathbf{h}}_S = \mathbf{m} \quad \text{with} \quad \mathbf{h}_S = \mathbf{I}_S\Omega_S \tag{9}$$

$\mathbf{h}_S$ is the angular moment of the system, $\mathbf{I}_S$ is the inertia tensor with respect to the center of mass and Ω_S is the angular velocity. The subscript $\dot{}$ refers to the time derivative. The total force acting in the body $\mathbf{f}$ is the resultant of gravity and the hydrodynamic interaction along the body surface which also produces $\mathbf{m}$; the external moment with respect to the center of mass. Moreover, m stands for the mass and $\mathbf{a}$ is the translational acceleration with the corresponding velocity noted as $\mathbf{v}$. The rotation matrix $\mathbf{R}$ and the body frame allow to rephrase the angular momentum equation equation above in a convective form, typically employed in rigid body mechanics (body coordinates) and suitable for the time stepping algorithm that we present later. We introduce below the convective angular momentum:

$$\mathbf{h} = \mathbf{J}\Omega = \mathbf{R}^{\mathrm{T}}\mathbf{h}_S \tag{10}$$

$\mathbf{J} = \mathbf{R}^{\mathrm{T}}\mathbf{I}_S\mathbf{R}$ is the constant tensor of inertia of the body and $\Omega = \mathbf{R}^{\mathrm{T}}\Omega_S$ is the angular velocity expressed in the convected frame, such that we have $\dot{\mathbf{R}}\mathbf{h} = \mathbf{m}$. The rotational equation of motion in the convected frame can be written:

$$\mathbf{J}\,\dot{\Omega} + \widetilde{\Omega}\mathbf{J}\,\Omega = \mathbf{m} \tag{11}$$

3 COMPUTATIONAL ALGORITHM

We propose a weakly-coupled algorithm that orchestrates well proved numerical algorithms for the different sub-problems: rigid body motion, moving domain, and fluid flow. A Predictor/Corrector approach, introduced in Dettmer and Perić (2012), is used and detailed in section

3.3. Subscripts $\hat{}$ and * are used to designate forces and moments respectively predicted and calculated in the time loop. The proposed numerical integration scheme corresponding to the evolution of the coupled system between time steps t_n and t_{n+1} and detailed in this section is summarized below:

Given $(\mathbf{u}, p)$ and $(\mathbf{x}, \mathbf{R})$ variables at $t = t_n$

1. Compute the force/moment estimation $(\hat{\mathbf{f}}^{n+1}, \hat{\mathbf{m}}^{n+1})$ using (20)
2. Compute the rigid body motion $(\mathbf{x}, \mathbf{R})_{t=t_{n+1}}$ solving (11).
3. Compute $\mathbf{u}_{mesh}^{n+1}$ solving the Boundary Value Problem (6) and the updated position of Γ_L
4. Solve the Navier-Stokes equation (5) to obtain $(\mathbf{u}, p)_{t=t_{n+1}}$
5. Compute the corrected force/moment $(\mathbf{f}^{n+1}, \mathbf{m}^{n+1})$ using (21)

End of the loop: $n \leftarrow (n+1)$

The nodal forces equivalent to the full stresses in the rigid bodies, measured in the surrounding elements are computed using (12), that is:

$$\mathbf{f}_{int}^{e} = \int_{\Omega_e} \mathbf{B}^T \, \sigma \, d\Omega_e \quad \text{with} \quad \mathbf{B} = B_{jI} = \frac{\partial N_I}{\partial x_j}, \quad I = 1, .., n_{elts} \tag{12}$$

Ω_e is the element domain, n_{elts} is the number of element nodes and N_I are the shape functions of an element. We consider in (12) only the elements meeting the condition $\Omega_e \subset \text{Adj}(\Gamma_L)$, $\text{Adj}(\Gamma_L)$ being the region spanning elements with at least one node lying in Γ_L. Finally, summing internal forces of each element, we obtain the resulting forces on the object

$$\mathbf{f}_n = -\mathbf{A}_e \mathbf{f}_{int}^{e} \mid_{\Gamma_L^e} \quad \text{with} \quad \Gamma_L^e = \Gamma_L \cap \Gamma^e \tag{13}$$

In (13), $\mathbf{A}_e$ is the standard finite element assembly operator restricted to Γ_L^e and Γ^e is the boundary of Ω_e. The hydrodynamic force $\mathbf{f}_*$ and the moment $\mathbf{m}_*$ applied on the immersed body are computed according the following relations:

$$\mathbf{f}_* = \sum_{j=1}^{n_L} \mathbf{f}_j \qquad \mathbf{m}_* = \sum_{j=1}^{Ne} \mathbf{r}_j \wedge \mathbf{f}_j \tag{14}$$

n_L is the number of nodes lying on the Lagrangian boundary and $\mathbf{r}_j$ are vectors between the center of mass of the rigid body and the application point of forces $\mathbf{f}_j$. In the rest, the index $n+i, i \in [\![-1; 1]\!]$ corresponds to the time step $n+i$ $(t = t_{n+i})$.

The flow solver, employs linear tetrahedra edge-based data structures and an advanced inexact nodal block-diagonal preconditioned Newton-Krylov solvers. An implicit predictor-multicorrector scheme is used for time-discretization and the resulting linear system is solved by an edge-based GMRES(m) method. For more details concerning the flow solver see Elias and Coutinho (2007); Elias et al. (2009); Lins et al. (2010). In the following subsections we discuss in more depth other crucial aspects of the present computational algorithm: (i) accurate rigid-body motion, (ii) coupling set-up, (iii) adaptive time-step control.

3.1 Translational movement

The generalized-α method is a well known and widely used scheme, it was originally developed by Chung and Hulbert Chung and Hulbert (1993). For particular values of those parameters, we obtain classical time integration schemes such as the mid-point rule, Newmark method, HHT method, etc. We choose here the implicit midpoint rule method (see Table 1), the different unknowns are expressed at time step $n+1/2$, and we consider the following values: $\gamma = \frac{1}{2}$ and $\beta = \frac{1}{4}$. $\mathbf{x}^{n+1}$ and $\mathbf{v}^{n+1}$ are given by the Newmark scheme Newmark (1959).

Table 1: Mid-point time updatings.

$m\mathbf{a}^{n+1/2}$	=	$\mathbf{f}^{n+1/2}$
$\mathbf{x}^{n+1}$	=	$\mathbf{x}^n + \Delta t\mathbf{v}^n + \Delta t^2\left(\left(\frac{1}{2}-\beta\right)\mathbf{a}^n + \beta\mathbf{a}^{n+1}\right)$
$\mathbf{v}^{n+1}$	=	$\mathbf{v}^n + \Delta t\left((1-\gamma)\,\mathbf{a}^n + \gamma\,\mathbf{a}^{n+1}\right)$
$\mathbf{f}^{n+1/2}$	=	$\left(\mathbf{f}^n + \mathbf{f}^{n+1}\right)/2$
$\mathbf{a}^{n+1/2}$	=	$\left(\mathbf{a}^n + \mathbf{a}^{n+1}\right)/2$

3.2 Rotational motion

Among the numerous contributions on the topic, we have to cite the fundamental articles of J. Simo and his coworkers who represented the rotations using the special orthogonal Lie group Simo and Vu-Quoc (1986, 1988). Cardona and Géradin then extended those works to flexible multibody dynamics Géradin and Cardona (1993). We will first present the parametrization of the problem, the equation of rotation and the time integration scheme used. For more details concerning the demonstrations see Géradin and Rixen (1995); Säfström (2009); Simo and Vu-Quoc (1988).

Parametrization, The Euler's theorem states that for any rotation matrix, we can associate an angle and an axis of rotation. The orthonormal property of $\mathbf{R}$ can be translated into 6 constraints and implies that $\mathbf{R}$ can be expressed using three parameters. Among the different ways of writing the rotation matrix, we chose the Rodrigues'formula Géradin and Rixen (1995) for its convenient expression. Let Ψ be the rotation vector associated to $\mathbf{R}$ such as $\Psi = \|\Psi\|\,\mathbf{n}_u$, $\mathbf{n}_u$ being a unit vector. $\widetilde{\mathbf{n}}_u$ is the skew-symmetric cross product matrix associated to the vector $\mathbf{n}_u = [n_1\ n_2\ n_3]^T$ such as, for an arbitrary vector $\mathbf{a}$: $\mathbf{n}_u \times \mathbf{a}$. The Rodrigues'formula gives:

$$\mathbf{R} = \mathbf{I} + \frac{\sin\|\Psi\|}{\|\Psi\|}\widetilde{\Psi} + \frac{1-\cos\|\Psi\|}{\|\Psi\|^2}\widetilde{\Psi}\widetilde{\Psi} \tag{15}$$

We can show that the matrix $\dot{\mathbf{R}}\mathbf{R}^T$ is skew symmetric writing the time derivative of $\mathbf{R}\mathbf{R}^T$. Then, as it is defined in Géradin and Rixen (1995), we introduce the matrix of angular velocity $\widetilde{\Omega}$ expressed in the material coordinates: $\widetilde{\Omega} = \mathbf{R}^T\dot{\mathbf{R}}$. Ω can be expressed as a function of Ψ using the mapping $\mathbf{T}$ Géradin and Rixen (1995); Mäkinen (2001):

$$\Omega = \mathbf{T}\dot{\Psi} \quad \text{and} \quad \text{with} \quad \mathbf{T} = \mathbf{I} + \left(\frac{\cos\|\Psi\|-1}{\|\Psi\|^2}\right)\widetilde{\Psi} + \left(1-\frac{\sin\|\Psi\|}{\|\Psi\|}\right)\frac{\widetilde{\Psi}\widetilde{\Psi}}{\|\Psi\|^2} \tag{16}$$

Compound Rotation, The compound rotation is defined using the left translation map of $SO(3)$, $\mathbf{R}_{incr}$ being an incremental rotation matrix, we have:

$$\mathbf{R}_{new} = \mathbf{R}\mathbf{R}_{incr} = \mathbf{R}\exp\left(\widetilde{\Theta}_{\mathbf{R}}\right) \tag{17}$$

$\widetilde{\Theta}_{\mathbf{R}}$ is the incremental rotation vector with respect to the base point $\mathbf{R}$ (in the remainder of this work, we will keep the notation $\widetilde{\Theta}$). $\widetilde{\Theta}$ corresponds to the material incremental rotation vector.

Time Integration Scheme, The problem of time stepping update can be formulated generalizing the results obtained in section 3.2. Given a configuration at time step n: $\mathbf{R}^n$, Ω^n, and $\mathbf{A}^n$, find the updated configuration $\mathbf{R}^{n+1} = \mathbf{R}^n \exp\left(\widetilde{\Theta}^n\right)$, Ω^{n+1}, and $\mathbf{A}^{n+1}$. In Cardona and Géradin (1988); Simo and Vu-Quoc (1988), the authors give the modified Newmark scheme for the orthogonal group $SO(3)$. As it is underlined in Akkerman, Dunaway, Kvandal, Spinks and Bazilevs (2012); Simo and Hughes (1998), this time integration scheme is appropriated when the rotation matrix is used to model the rotation of the rigid body motion. Due to its properties of stability, also presented for the translational movement, the mid-point scheme is preferred. For incremental force free motion, this scheme exactly conserves the energy Simo and Wong (1991). Expressing (9) at time step $n+1/2$, the discrete conservation law $\dot{\mathbf{h}}_S^{n+1/2} = \mathbf{M}^{n+1/2}$ can be written as:

$$\mathbf{R}^{n+1}\mathbf{J}\Omega^{n+1} - \mathbf{R}^n\mathbf{J}\Omega^n - \Delta t\mathbf{M}^{n+1/2} = \mathbf{G}(\Theta^n) = 0 \tag{18}$$

To solve this nonlinear equation by Newton's method, we have to linearize $\mathbf{G}(\Theta^n)$ around an intermediate step i between n and $n+1$ and in the direction $\Delta\Theta^n_{(i)} = \Theta^n_{(i+1)} - \Theta^n_{(i)}$. After linearization we can express the tangent matrix using the operator $\mathbf{T}$ introduced in (16) at every subiterative steps (see Simo and Wong (1991)):

$$\mathbf{K}^{n+1}_{(i)}\Delta\Theta^n_{(i)} = \mathbf{Re}_{(i)} \quad \text{with} \quad \mathbf{K}^{n+1}_{(i)} = \mathbf{R}^{n+1}_{(i)}\left[\frac{\gamma}{\Delta t\beta}\mathbf{J}\mathbf{T}_n - \widehat{\mathbf{J}\Omega}^{n+1}_{(i)}\right] \tag{19}$$

$\mathbf{K}^{n+1}_{(i)}$ and $\mathbf{Re}_{(i)}$ are the tangent matrix and residual. Considering the midpoint rule method as it has been introduced with the translational motion, the initial and interation variables are given in Table 2 and 3.

Table 2: Initial variables

$\Theta^n_{(0)}$	=	$\Delta t\Omega^n + \frac{\Delta t}{4}\mathbf{A}^n$
$\mathbf{R}^{n+1}_{(0)}$	=	$\mathbf{R}^n\exp\left(\widetilde{\Theta}^n_{(0)}\right)$
$\Omega^{n+1}_{(0)}$	=	$\Omega^n + \frac{\Delta t}{2}\mathbf{A}^n$

At the beginning of the sub-iteration, the residual $\mathbf{Re}_{(0)} = \mathbf{R}^{n+1}_{(0)}\mathbf{J}\Omega^{n+1}_{(0)} - \mathbf{R}^n\mathbf{J}\Omega^n - \Delta t\mathbf{M}^{n+1/2}$ is computed for a convergence check (see Table 2). With (19) we obtain the increment $\Delta\Theta^n_{(i)}$ and the iteration variables with Table 3. For the test cases presented in section 4 we notice that one to two sub-iterations are enough to converge. Variables increment is made once the

Table 3: Iteration variables

$\Delta\Theta^{n}_{(i)}$	=	$\left[\mathbf{K}^{n+1}_{(i)}\right]^{-1}\mathbf{Re}_{(i)}$
$\mathbf{R}^{n+1}_{(i+1)}$	=	$\mathbf{R}^{n}\exp\left(\widetilde{\Theta}^{n}_{(i+1)}\right)$
$\exp\left(\widetilde{\Theta}^{n}_{(i+1)}\right)$	=	$\exp\left(\widetilde{\Theta}^{n}_{(i)}\right)\exp\left(\Delta\widetilde{\Theta}^{n}_{(i)}\right)$
$\Omega^{n+1}_{(i+1)}$	=	$\Omega^{n+1}_{(i)}+\frac{\gamma}{\Delta t\beta}\Delta\Theta^{n}_{(i)}$

Table 4: Variables increment

$\mathbf{R}^{n+1}$	=	$\mathbf{R}^{n+1}_{(m_f)}$
Ω^{n+1}	=	$\Omega^{n+1}_{(m_f)}$
$\mathbf{A}^{n+1}$	=	$\frac{\Omega^{n+1}-\Omega^{n}}{\Delta t\gamma}+(1-\frac{1}{\gamma})\mathbf{A}^{n}$

convergence is reach. Writing m_f the number of subiteration required between time step n and $n+1$, Table 4 gives the expression of the unknowns at time step $n+1$.

We adapt in the remainder of this work this algorithm first presented in Simo and Wong (1991) when the external efforts $(\mathbf{f}^{n+1}, \mathbf{M}_{n+1})$ have to be estimated (weak coupling). In section 3.3 we present the chosen method for the Prediction/Correction of these unknowns.

3.3 Coupling Set up

The weak coupling between the equations is allowed via data exchange through boundary conditions. The algorithm used does not provide the force at time step $n+1$ as the body equation is solved first. As reminded in Akkerman, Bazilevs, Benson, Farthing and Kees (2012), a limit of the staggered schemes is when the time step increases. On the other hand, they allow the use of sub-solver softwares such as the VOF method. In Dettmer and Perić (2012), the authors also underline the fact that in the case of an incompressible fluid-structure interaction staggered schemes proposed in literature are not suitable and propose a staggered scheme using a predictor-corrector approach giving good results. The Force/Moment applied on the Fluid-Object interface is first predicted:

$$\begin{pmatrix}\mathbf{f}^{n+1}\\ \mathbf{m}^{n+1}\end{pmatrix}\approx\begin{pmatrix}\hat{\mathbf{f}}^{n+1}\\ \hat{\mathbf{m}}^{n+1}\end{pmatrix}=(1+\tau)\begin{pmatrix}\mathbf{f}^{n}\\ \mathbf{m}^{n}\end{pmatrix}-\tau\begin{pmatrix}\mathbf{f}^{n-1}\\ \mathbf{m}^{n-1}\end{pmatrix} \tag{20}$$

$(\hat{\mathbf{f}}^{n+1}, \hat{\mathbf{m}}^{n+1})$ are the predicted Force / Moment. For $\tau = 1$ and a fixed time step we have a first order Newton-Gregory backward polynomial Cellier and Kofman (2006) and for $\tau = 0$ the backward Euler method. If $\tau = 0$ the impact of the fluid on the solid is ignored. In a general case, with variable time step, the parameter τ is set as $\tau = \Delta t_{n+1}/\Delta t_n$.
Using the notation $(\mathbf{f}^{n+1}_{*}, \mathbf{m}^{n+1}_{*})$ for the Force / Moment computed after solving the incompressible fluid flow equation (1) (once $\mathbf{x}^{n+1}$ and Θ^{n} are known), the corrected Force / Moment $(\mathbf{f}^{n+1}, \mathbf{m}^{n+1})$ are given as:

$$\begin{pmatrix}\mathbf{f}^{n+1}\\ \mathbf{m}^{n+1}\end{pmatrix}=\tau_*\begin{pmatrix}\mathbf{f}^{n+1}_{*}\\ \mathbf{m}^{n+1}_{*}\end{pmatrix}+(1-\tau_*)\begin{pmatrix}\hat{\mathbf{f}}^{n+1}\\ \hat{\mathbf{m}}^{n+1}\end{pmatrix} \tag{21}$$

The parameter τ_* has to be set and a natural choice is $\tau_* = 1/2$. If $\tau_* = 0$ the impact of the fluid on the solid is ignored. Small values of τ_* reduces the impact of added mass effect and allows to achieve unconditional stability Dettmer and Perić (2012). In section 4.3, we illustrate the role those parameters can have in particular cases.

3.4 Time step control

Proportional-Integral-Derivative (PID) controllers are extensively used in canonical control applications Gustafsson, Lundh and Soderlind (1988). The advantageous performances of PID strategy for general coupled problems are presented in Valli, Carey and Coutinho (2002, 2005). Among the possible control forms we consider here the Courant-Friedrichs-Lewy number (CFL) that is directly linked with the time step calculation:

$$\Delta t_{n+1} = \min_{\Omega_e}\left(\frac{h_e}{\|\mathbf{u}_{n+1}(\Omega_e)\|}\right)\mathrm{CFL}_{n+1} \quad \text{with} \quad \frac{\mathrm{CFL}_{n+1}}{\mathrm{CFL}_n} = \left(\frac{e_{n-1}}{e_n}\right)^{k_P}\left(\frac{1}{e_n}\right)^{k_I}\left(\frac{e_{n-1}^2}{e_n\, e_{n-2}}\right)^{k_D} \tag{22}$$

e_n is the measure of the normalized change of the quantities of interest in time step n. Here, the fluid velocity and pressure are used and we have:

$$e_n = \frac{e_U}{\mathrm{Tol}_U} \quad \text{with} \quad e_U = \frac{\left\|\mathbf{U}_n^P - \mathbf{U}_{n-1}^G\right\|}{\left\|\mathbf{U}_n^G\right\|} \tag{23}$$

Tol_U is the tolerance considered and $\mathbf{U}_n^G$ is the vector containing the velocity and pressure for the fluid domain at time step n. To prevent an excessive growth or reduction of the step in the controller, minimum and maximum values are set, which limit the control signal (anti-windup effect G.F., J.D. and A. (1994)): $\mathrm{CFL}_{min} \leq \mathrm{CFL}_{n+1} \leq \mathrm{CFL}_{max}$. For different test problems, parametric studies were performed for different values of (k_P, k_I and k_D), to verify the robustness of the PID controller Valli, Carey and Coutinho (2005). The controller was found to be very robust, allowing us to fix the values of the PID parameters, $k_P = 0.075$, $k_I = 0.175$ and $k_D = 0.01$, for all the numerical experiments described in Valli et al. (2009). Considering equation (22) we notice that the parameter $\tau = \Delta t_{n+1}/\Delta t_n$, introduced in (21) for the external force and torque calculation of the rigid body equation, is directly linked with the controller used and thus the velocity and pressure in the fluid, and also the mesh movement.

4 NUMERICAL SIMULATIONS

4.1 Vortex Induced Vibration: 2D flow

A rigid plate is placed under an incompressible fluid flow with a torsional stiffness and damping on its center of mass. This test case is widely used, especially to study the rotational and translational galloping instabilities or vortex induced vibrations (VIV). Those instabilities may occur when the vortex shedding frequency is close to the natural frequency of the plate-torsion spring system. We focus on the rotational movement, translational movements are blocked and the plate can only rotates around its center of mass and according to the axis $\mathbf{e}_y$

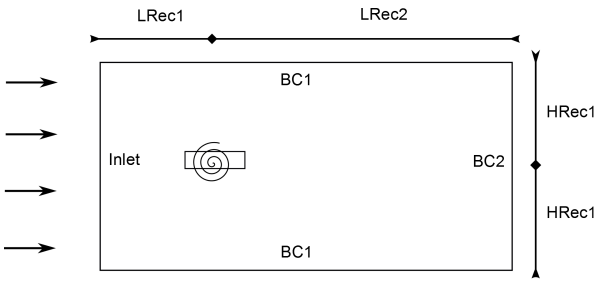

Figure 1: Scheme of the $2D$ problem. In meters, $LRec1 = 25$ m, $LRec2 = 55$ m, $HRec1 = 30$ m. Length of the plate: $L = 4$ m and its thickness $h = 1$ m.

perpendicular to the plane of study ($(\mathbf{e}_x, \mathbf{e}_y, \mathbf{e}_z)$ are the vector basis of the inertial frame), the setup is presented in Fig. 1.

In Robertson et al. (2003) and Li, Sherwin and Bearman (2000), a weak coupling using the ALE framework is considered for this test case. The references Dettmer and Perić (2006); Hesch et al. (2014); Yang and Stern (2012) propose a strong coupling approach using respectively a mortar method, a simplified embedded-boundary formulation and a Newton-Raphson method. Only the 2D problem is presented in the literature and our solver *EdgeCFD* is 3D. We create a 3D geometry with a depth $L_y = 1$ m in order to compare with existing results and use the same values for the parameters. The *inlet* boundary condition is given by the normal velocity $U = \mathbf{u} \cdot \mathbf{e}_x$ of the fluid. The boundary condition $BC1$ on the upper and bottom part of the fluid domain corresponds to $\mathbf{u} \cdot \mathbf{e}_z = 0$, and we have $p = 0$ for $BC2$. The non slip boundary condition is applied on the solid. To characterize the numerical experiments we introduce the mass moment of inertia ratio $I_n = I/(\rho h^4)$ where I and h are the moment of inertia according to $\mathbf{e}_y$ and h is the thickness of the plate. Δ is the ratio between the length of the plate and h. We also define the reduced velocity $U_R = U/(f_n h)$, f_n being the natural frequency of the system such as $f_n = \frac{1}{2\pi}\sqrt{k/I}$. k is the torsional stiffness constant and ξ is the damping ratio: $\xi = c/2\sqrt{k\,I}$ where c is the damping coefficient. The Reynolds number Re is defined as $Re = Uh/\nu$, ν being the kinematic viscosity. We consider here three different fluid meshes ($M1$, $M2$, $M3$) with respectively a mesh size on the Fluid-Object interface Γ of 0.08 m, 0.06 m, and 0.04 m and a total of 39, 967 for $M1$, 59, 598 for $M2$ and 115, 788 tetrahedral elements for $M3$. The ratio between the mesh size on Γ and on the inlet surface is respectively 43.75, 58.33 and 87.5.

To evaluate the formulation given in sections 2 and 3, we consider parameters that allow a comparison with other studies Dettmer and Perić (2006); Hesch et al. (2014); Robertson et al. (2003); Yang and Stern (2012): $U_R = 40$, $Re = 250$, $\xi = 0.25$, $I_n = 400$, $f_n = 0.0625$ (Hz), $\Delta = 4$ and $L_y = 1$ m. We also consider the three fluid meshes $M1$, $M2$ and $M3$ for different time steps Δt between 8×10^{-4} (s) and 7×10^{-2} (s). Usually in the literature, the mesh size is taken between 0.033 m and 0.067 m on the Fluid-Object interface. The ratio between the natural frequency and the observed oscillation frequency of the plate f_n/f_o and the amplitude of the oscillation is given in Table 5 for the RBVMS formulation. Here, the frequency is calculated considering the signal after the plate reaches its maximum amplitude rotation. The results found in the literature are within the interval [0.76, 0.78] with an amplitude between 0.2269 to 0.2618 radians Hesch et al. (2014).

Table 5: Values of the ratio f_o/f_n, for different time steps, mesh size. M.D. indicates a calculation that could not end due to a local excessive mesh deformation.

Δt (s)	RBVMS					
	M1		M2		M3	
	f_o/f_n	$\theta_Y^{max}(rad)$	f_o/f_n	$\theta_Y^{max}(rad)$	f_o/f_n	$\theta_Y^{max}(rad)$
8×10^{-4}	0.802	0.2407	-	-	-	-
10^{-3}	0.7936	0.2409	0.7328	0.2398	M.D.	M.D.
5×10^{-3}	0.7808	0.2377	0.7808	0.2358	M.D.	M.D.
10^{-2}	0.7808	0.2344	0.7808	0.2334	0.7808	0.2374
5×10^{-2}	0.8	0.1911	M.D.	M.D.	0.7808	0.2354
7×10^{-2}	0.7808	0.1857	-	-	-	-

The frequency ratio is stable but the maximum amplitude tends to reduce when the time step increases. Those results are in a good agreement with those presented in the literature. The parameter τ_{mesh} computed at every time step (see (7)) induces a stiffening effect that is inversely proportional to the element volume. Small elements displacement is the highest and we notice that the maximum CFL number is in the vicinity of the plate. We can also notice that a reduction of the time step does not guaranty a better result and can lead to local excessive mesh distortion.

4.2 Variable time step

We now consider the use of a variable time step (see section 2) controlled by the CFL number that takes into account the time step and mesh size. Examples of calculations using a variable time step is given by Fig. 2. For the calculations with variable time step, the tolerance Tol_U in (23) is fixed at 0.04. As it has been presented in section 3.4, we force the CFL number to be within an certain interval. Different intervals have been tested including a calculation with a small interval centered around the value 1. A comparison is made with a calculation of reference with a fixed time step $\Delta t = 0.005$ (s).

The results with the variable time step are in a good agreement with the reference calculation. The minimum CFL condition has little influence on the signal but the transient phase of the calculation with a CFL number forced to 1 is strongly different from the fixed time step calculation. This anomaly can be explained looking at the time step computed at the beginning of the calculation. When the CFL number is forced into the intervals [0.3; 1] and [0.5; 1] the time step for the first seconds is around 0.003 s and 0.005 s respectively, while the time step when the CFL number is in [0.95; 1.05] is around 0.01 s. The minimum CFL number has to be set small enough to give good results. If around 80000 steps are necessary to reach 400 s for the fixed time step, 37000 and 36600 are necessary for the calculations with a CFL number in [0.3; 1] and [0.5; 1] respectively.

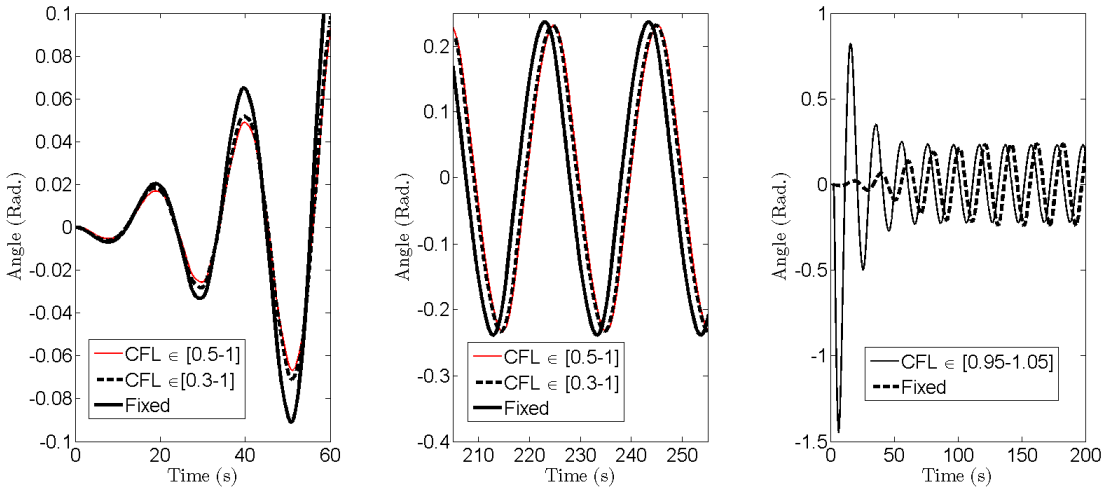

Figure 2: Influence of the CFL range for variable time step with $I_n = 400$, $U_R = 40$, $Re = 250$, $k = 61.685$ ($\mathbf{M.m}^{-1}$), $\xi = 0.25$, RBVMS method.

4.3 Parametric study for the Fluid-Object coupling

As described in section 3.3, two parameters (τ, τ_*) are used to compute the force/moment prediction $(\hat{\mathbf{f}}^{n+1}, \hat{\mathbf{m}}^{n+1})$ at the beginning of the time loop and the force/moment correction $(\mathbf{f}^{n+1}, \mathbf{m}^{n+1})$ at the end.

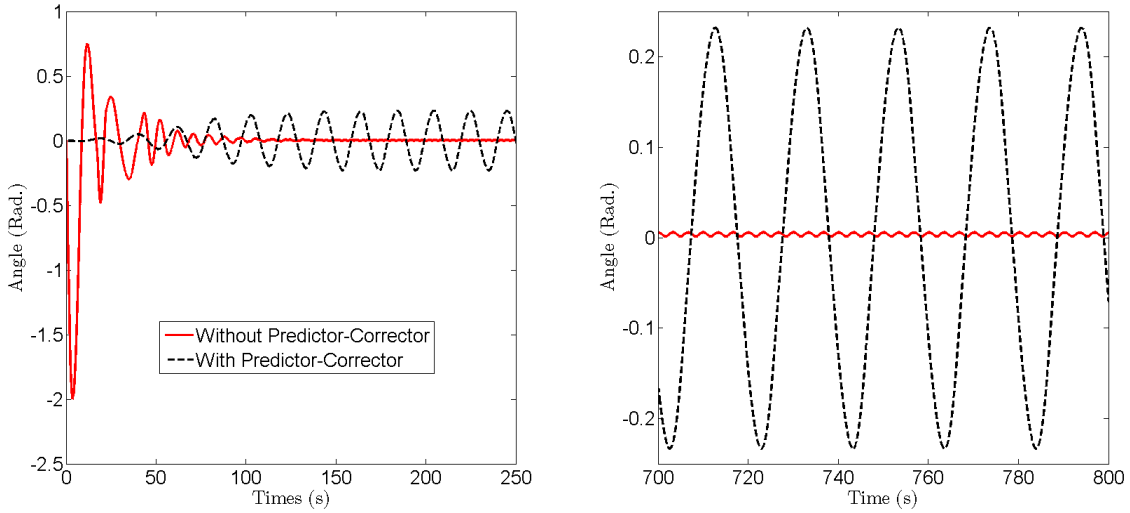

Figure 3: Comparison for a variable time step (CFL within the range $0.5 - 1$) of the response with and without force prediction. $I_n = 400$, $U_R = 40$, $Re = 250$, $k = 61.685$ ($\mathbf{M.m}^{-1}$), $\xi = 0.25$, mesh $M1$, RBVMS method.

Fig. 3 and 4 illustrate the role those parameters can have in particular cases. In Fig. 3, two calculations with variable time step are compared. A calculation using a predicted and corrected force/moment with parameters $(\tau, \tau_*) = (1, 1/2)$ that have been presented in Fig. 2 and the other one without prediction or correction which is equivalent to consider $(\mathbf{f}^{n+1}, \mathbf{m}^{n+1}) = (\mathbf{f}^n_*, \mathbf{m}^n_*)$. We notice that a calculation without an estimation of the fluid load

for a variable time step gives non-coherent solution in comparison with the signal of reference in terms of transient signal and for the maximum amplitude at the permanent oscillatory state.

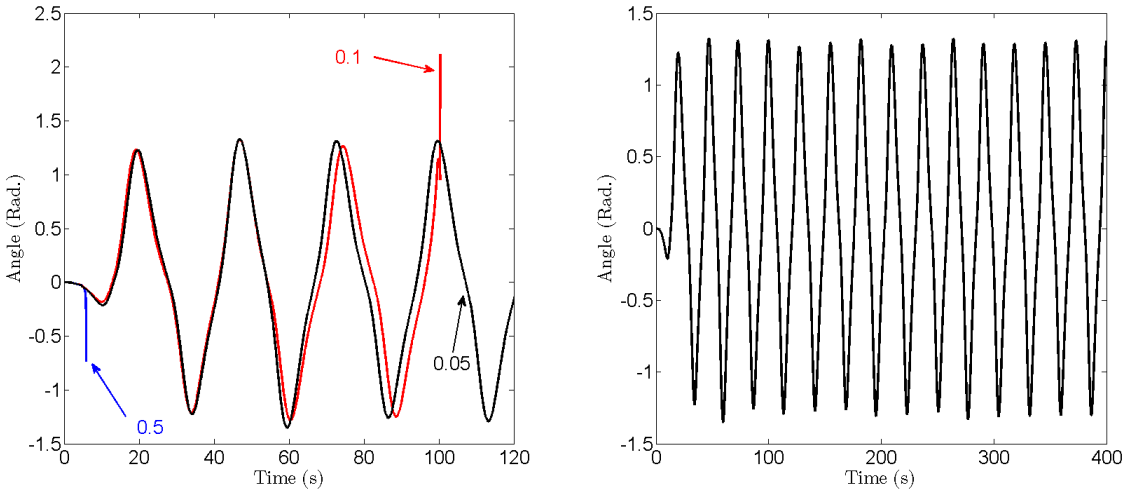

Figure 4: Influence of the parameter τ_*. $I_n = 200$, $U_R = 40$, $k = 30.84$ (M.m^{-1}), $\xi = 0.25$, mesh $M1$, Fluid density: 2.5 kg/m3, RBVMS method with fixed time step: $\Delta t = 5 \times 10^{-2}$ s. On the left, a superposition of the response for the first 140 seconds for $\tau_* = 0.5$, $\tau_* = 0.1$, $\tau_* = 0.05$. On the right, the response for $\tau_* = 0.05$.

The second example shows the influence of the parameter τ_* used to compute the corrected force and moment. As presented in Dettmer and Perić (2012) this parameter can be reduced to achieve unconditional stability in case of small ratio between the solid and fluid mass (when added mass effect can occur). In Fig. 4 we consider a test case increasing the fluid density and reducing the moment of inertia of the rigid body. We can see that the usual value $\tau_* = 1/2$ does not give satisfying results as the signal diverges leading to mesh distortions that stop the calculation after few seconds. Reducing the parameter and considering $\tau_* = 1/10$ improves the result and we have a signal with high amplitudes that reaches 100 seconds of calculation and then stops for the same reasons. keeping reducing the parameter τ_* with $\tau_* = 1/20$ gives a good result with stable oscillations and for a long-range calculation.

4.4 3D rotations

One of the advantages of the formulation presented is its capability to treat any kind of geometry and in particular 3D problems. Fig. 6 illustrates a calculation inspired by the 2D problem in section 4.1, a unit cube with 3 rotational degrees of freedom is placed under a fluid flow. Three identical torsion springs are considered for each rotational degree of freedom. The geometry presented in Fig. 6 has 25994 nodes and 139092 tetrahedral elements. The inlet face is a square of side 30 m. Three identical torsional springs are used for each spatial direction. Boundary conditions are the same as those presented in Fig. 1. Here $LRec1 = 25$ m and $LRec2 = 55$ m.

Fig. 5 gives the angle of rotation obtain summing the incremental angles Θ^n expressed in Table 3 in the body frame $\mathbf{B}_{body} = \{\mathbf{b}_x, \mathbf{b}_y, \mathbf{b}_z\}$ for every direction. Snapshots of the simulation

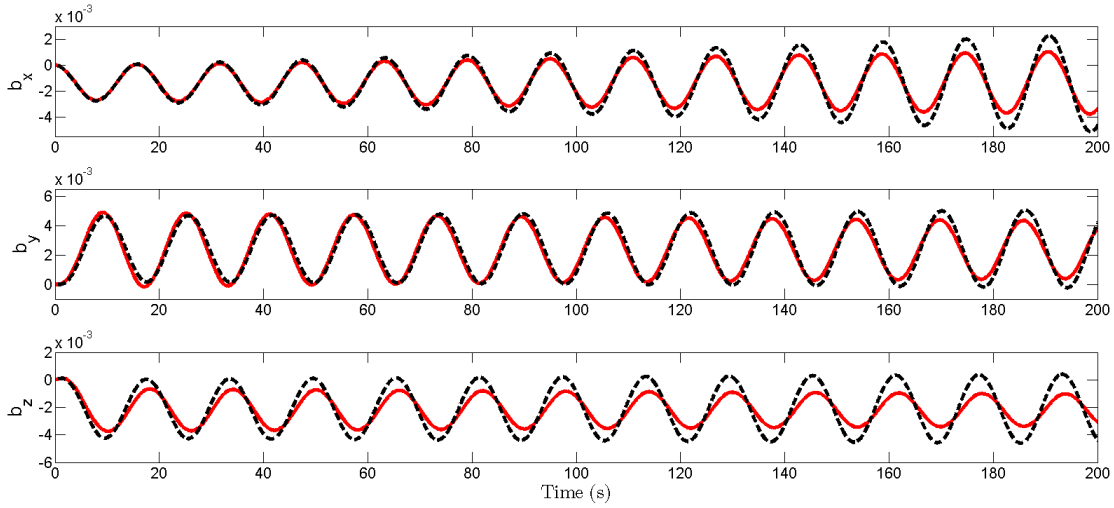

Figure 5: Oscillations (in degrees) of a cube with 3 degrees of freedom (rotations) for a fixed (continuous line) and variable time step (dashed line). $U_R = 40$**,** $\xi = 0$**,** $I_n = 100$**,** $k = 15, 42$ **(M.m^{-1}),** $Re = 250$**. From the top to the bottom: axis b$_x$, b$_y$ and b$_z$. RBVMS Method**

Table 6: Statistics of the calculations with fixed and variable time step for a cube with three degrees of freedom (rotations).

	Variable Time Step	Fixed Time Step $\Delta t = 10^{-2}$ (s)
Number of time steps	16,583	20,000
Number of Inexact Newton Method iterations	69,240	82,312
CFL max	0.85	0.65

are given in Fig. 6 where velocity streamlines are plotted around the cube.
In Table 6, statistics of the calculations are given. We compare the total number of non linear iterations between the fixed and variable time step calculation, done at every time step for the Inexact Newton Solver (fluid equation) and the maximum CFL for the overall simulation. For the variable time step, the time step (in seconds) varies with the interval [0.0019; 0.0131].

The variable time step solution diminishes the number of steps and nonlinear iterations, respecting the imposed CFL condition and consequently improving the computational time.

5 CONCLUSION

A fully three dimensional coupling between a rigid body immersed in a fluid has been presented. A staggered scheme has been used here and we considered a predictor / corrector approach with time step control. The role of each parameters used and the advantages of the time step control have been illustrated. The coupling set up used has been applied on test cases with an incompressible fluid flow. This complex configuration is treated within the ALE framework.

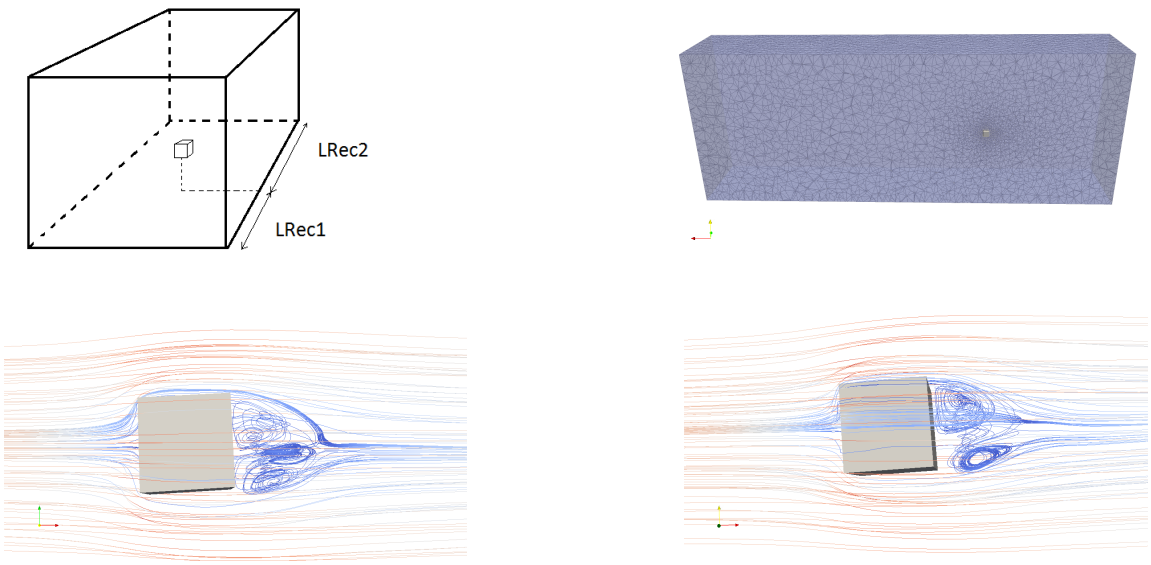

Figure 6: From the top to the bottom and the left to the right: Scheme of the test case, representation of the cube and half the fluid mesh, snapshots with velocity streamlines around the cube for the 3D simulation: $(\mathbf{e}_z, \mathbf{e}_x)$ plane view, $(\mathbf{e}_y, \mathbf{e}_x)$ plane view.

Focusing on the FSI part of the problem and especially the rotational movement, we have presented a comparison when the fluid is treated by RBVMS. Good results have been obtain in the context of Vortex Induced Vibration in comparison with the literature. These results represent a basis for future works on FOI with free surface, as the staggered scheme presented is well adapted to include the computation of the VOF equation.

ACKNOWLEDGEMENTS

This work is partially supported by CAPES, CNPq and FAPERJ. EdgeCFD has been developed in the High Performance Computing Center of COPPE/Federal University of Rio de Janeiro for Petrobras S.A.

REFERENCES

Akkerman, I., J. Dunaway, J. Kvandal, J. Spinks and Y. Bazilevs. 2012. "Toward free-surface modeling of planing vesels: simulation of the Fridsma hull using ALE-VMS." *Computational Mechanics* 50:719–727.

Akkerman, Ido, Y Bazilevs, DJ Benson, MW Farthing and CE Kees. 2012. "Free-surface flow and fluid-object interaction modeling with emphasis on ship hydrodynamics." *Journal of Applied Mechanics* 79(1):010905.

Bazilevs, Y., Ming-Chen Hsu, Kenji Takizawa and T. E. Tezduyar. 2012. "ALE-VMS and ST-VMS methods for computer modeling of wind-turbine rotor aerodynamics and fluid-structure interaction." *Mathematical Models and Methods in Applied Sciences* 22.

Bazilevs, Y., V.M. Calo, J.A. Cottrell, T.J.R. Hughes, A. Reali, and G. Scovazzi. 2007. "Variational multiscale residual-based turbulence modeling for large eddy simulation of incompressible flows." *Comput. Methods Appl. Mech. Engrg.* 197:173–201.

Bazilevs, Yuri, Kenji Takizawa and Tayfun E. Tezduyar. 2013. *Computational Fluid-Structure Interaction Methods and Applications*. Wiley-Blackwell.

Calderer, R. and A. Masud. 2012. "A variational multiscale stabilized formulation for the incompressible NavierStokes equations." *Computational Mechanics* 44:146–160.

Calderer, Ramon and Arif Masud. 2010. "A multiscale stabilized ALE formulation for incompressible flows with moving boundaries." *Computational Mechanics* 46(1):185–197.

Calo, V. M. 2004. Residual-based multiscale turbulence modeling: finite volume simulations of bypass transition. PhD thesis Stanford University.

Cardona, A. and M. Géradin. 1988. "A beam finite element non-linear theory with finite rotations." *Int. J. Numer. Methods Engrg* 26:2403–2438.

Cellier, François E and Ernesto Kofman. 2006. *Continuous system simulation*. Springer Science & Business Media.

Chung, J. and G.M. Hulbert. 1993. "A time integration algorithm for structural dynamics with improved numerical dissipation: the generalized-α method." *Journal of Applied Mechanics* 60:371–375.

Codina, R. 2002. "Stabilized finite element approximation of transient incompressible flows using orthogonal subscales." *Computer Methodos in Appled Mechanics and Engineering* 191:42954321.

Codina, R., J. Principe and M. Avila. 2010. "Finite Element Approximation of Turbulent Thermally Coupled Incompressible Flows with Numerical Sub-grid Scale Modelling." *International Journal of Numerical Methods for Heat and Fluid Flow* 20:492516.

Day, A.H., A. Babarit, A. Fontaine, Y.-P. He, M. Kraskowski, M. Murai, I. Penesis, F. Salvatore and H.-K. Shin. 2015. "Hydrodynamic modelling of marine renewable energy devices: A state of the art review." *Ocean Engineering* 108:46–69.

Dettmer, W. and D. Perić. 2006. "A computational framework for fluid-rigid body interaction: Finite element formulation and applications." *Computer Methods in Applied Mechanics and Engineering.* 195:1633–1666.

Dettmer, Wulf G. and Djordje Perić. 2012. "A new staggered scheme for fluid-structure interaction." *Internal journal for numerical methods in engineering* .

Donea, Jean and Antonio Huerta. 2003. *Finite Element Methods for Flow Problems*. Wiley.

Elias, R. N. and A. L. G. A. Coutinho. 2007. "Stabilized edge-based finite element simulation of free-surface flows." *International Journal for Numerical Methods in Fluids* 54:965–993.

Elias, R.N., M. A.Gonçalves, A. L. G. A. Coutinho, P.T.T. Esperança, M.A.D. Martins and M.Ferreira. 2009. Free-surface flow simulation using stabilized edge-based finite element methods. In *In Proceeedings of ASME 2009 28th International Conference on Offshore Mechanics and Arctic Engineering OMAE, ASME*.

Géradin, M. and A. Cardona. 1993. Finite Element modeling concepts in multibody dynamics. In *Computer aided analysis of rigid and flexible mechanical systems*.

Géradin, Michel and Daniel Rixen. 1995. "Parametrization of finite rotations in computational dynamics: a review." *Revue européenne des éléments finis* 4:497–553.

G.F., Franklin, Powell J.D. and Emami-Naeini A. 1994. *Feedback Control of Dynamic Systems*. Addison-Wesley Publishing.

Gravemeier, V. and W.A. Wall. 2011. "Residual-based variational multiscale methods for laminar, transitional and turbulent variable-density flow at low Mach number." *International Journal for Numerical Methods in Fluids* 65:1260–1278.

Gustafsson, K., M. Lundh and G. Soderlind. 1988. "A PI stepsize control for the numerical solution for ordinary differential equations." *BIT* 28:270287.

Hesch, C., A.J. Gil, A. Arranz Carre no, J. Bonnet and J. Betsch. 2014. "A mortar approach for Fluid-Structure interaction problems: Immersed strategies for deformable and rigid bodies." *Comput. Methods Appl. Mech. Engrg* 278:853–882.

Hughes, T. J. R. 2012. *The finite element method: linear static and dynamic finite element analysis*. Courier Dover Publications.

Hughes, T.J.R., G.R. Feijoo, L. Mazzei and J.-B. Quincy. 1998. "The variational mulsticale method - a paradigm for computational mechanics." *Computer Methods in Applied Mechanics and Engineering* 166:3–24.

Li, L., S.J. Sherwin and P.W. Bearman. 2000. "A moving frame of reference algorithm for fluid/structure interaction of rotating and translating bodies." *International journal for numerical methods in fluids* pp. 1–20.

Lins, E.F., R.N. Elias, F.A. Rochinha and A.L.G.A. Coutinho. 2010. "Residual-based variational multiscale simulation of free surface flows." *Computational Mechanics* 46:545557.

Löhner, Rainald. 2008. *Applied computational fluid dynamics techniques: an introduction based on finite element methods*. John Wiley & Sons.

Mäkinen, Jari. 2001. "Critical study of Newmark-Scheme on manifold of finite rotations." *Computer methods in applied mechanics and engineering* 191:817–828.

Masud, Arif, Manish Bhanabhagvanwala and Rooh A Khurram. 2007. "An adaptive mesh rezoning scheme for moving boundary flows and fluid–structure interaction." *Computers & fluids* 36(1):77–91.

Masud, Arif and Thomas JR Hughes. 1997. "A space-time Galerkin/least-squares finite element formulation of the Navier-Stokes equations for moving domain problems." *Computer Methods in Applied Mechanics and Engineering* 146(1):91–126.

Miras, T., F. A. Rochinha, R. N. Elias, A. L. G. A. Coutinho, J. L. D. Alves and C. E. Silva. 2015. Simulating Highly Nonlinear Ship-Wave Interaction with EdgeCFD. In *Conference CILAMCE*. Rio de Janeiro: .

Newmark, N.M. 1959. "A Method of Computation for Structural Dynamics." *ASCE Journal of Engineering Mechanics Division* 85.

Principe, J., R. Codina and F. Henke. 2010. "The dissipative structure of variational multiscale

methods for incompressible flows." *Computer Methods in Applied Mechanics and Engineering* 199:791801.

Rasthofer, U. and V. Gravemeier. 2013. "Multifractal subgrid-scale modeling within a variational multiscale method for large-eddy simulation of turbulent flow." *Journal of Computational Physics* 234:79–107.

Robertson, I., L. Li, S.J. Sherwin and P.W. Bearman. 2003. "A numerical study of rotational and transverse galloping rectangular bodies." *Journal of Fluids and Structures* 17:681–699.

Säfström, Niklas. 2009. Modeling and simulation of rigid body and rod dynamics via geometric methods PhD thesis NTNU.

Simo, J.C. and K. K. Wong. 1991. "Unconditionally stable algorithms for rigid body dynamics that exactly preserve energy and momentum." *International journal for numerical methods in engineering* 31:19–52.

Simo, J.C. and L. Vu-Quoc. 1986. "A three-dimensional finite-stain rod model, part 2: Computational aspects." *Computer methods in applied mechanics and engineering* 58:79–116.

Simo, J.C. and L. Vu-Quoc. 1988. "On the dynamics in space of rods undergoing large motions - a geometrically exact approach." *Computer methods in applied mechanics and engineering* 66:125–161.

Simo, J.C. and T.J.R. Hughes. 1998. *Computational Inelasticity*. Springer-Verlag New York.

Souli, M'hamed and David J Benson. 2013. *Arbitrary Lagrangian Eulerian and Fluid-Structure Interaction: Numerical Simulation*. John Wiley & Sons.

Sung, H. Gun, H. Baek, S. Hong and J.-S. Choi. 2015. "Numerical study of vortex-induced vibration of pivoted cylinders." *Ocean Engineering* 93:98–106.

Tezduyar, T. E. 2007. "Finite elements in fluids: Stabilized formulations and moving boundaries and interfaces." *Computers and Fluids* 36:191–206.

Tezduyar, T. E., S. Mital, S. E. Ray and R. Shi. 1992. "Incompressible flow computations with stabilized bilinear and linear equal-order-interpolation velocity-pressure elements." *Comput. Methods Appl. Mech. Engrg* 95:221–242.

Tumkur, Ravi Kumar R., Ramon Calderer, Arif Masud, Arne J. Pearlstein, Lawrence A. Bergman and Alexander F. Vakakis. 2013. "Computational study of vortex-induced vibration of a sprung rigid circular cylinder with a strongly nonlinear internal attachment." *Journal of Fluids and Structures* 40:214–232.

Valli, A.M.P., G.F. Carey and A.L.G.A. Coutinho. 2002. "Control strategies for timestep selection in simulation of coupled viscous flow and heat transfer." *Communications in Numerical Methods in Engineering* 18:131–139.

Valli, A.M.P., G.F. Carey and A.L.G.A. Coutinho. 2005. "Control strategies for timestep selection in FE simulation of incompressible flows and coupled reactionconvectiondiffusion processes." *Int J Numer Methods Fluids* 47:201–231.

Valli, A.M.P., R.N. Elias, G.F. Carey and A.L.G.A. Coutinho. 2009. "PID adaptive control of

incremental and arclength continuation in nonlinear applications." *Int J Numerical Methods in Fluids* 61:11811200.

Yang, Jianming and Frederick Stern. 2012. "A simple and efficient direct forcing immerse boundary framework for fluid-structure interactions." *Journal of computational Physics* 231:5029–5061.